ELSEVIER

Physica C 245 (1995) 143–150

PHYSICA C

Enhancement of critical current and magnetic field in a defected Josephson tunneling junction

T.C. Chow [a,*], H. Chou [a], H.G. Lai [a], C.C. Liu [a], Y.S. Gou [b]

[a] *Department of Physics, National Sun Yat-Sen University, Kaohsiung, Taiwan*
[b] *Department of Electrophysics, National chaio Tung University, Hsin-Chu, Taiwan*

Received 28 October 1994

Abstract

A Josephson junction with a length of 10 times the Josephson penetration depth (λ_J) and a defect size of 0.5 λ_J to 2 λ_J in different positions has been studied by a mechanical simulation. It was found that the defect modulated the current distribution tremendously when it was near the edge of the junction. A surprising enhancement of the critical current under the field was observed when the defect was located at 0.5 λ_J and had a size from 0.5 λ_J to 2 λ_J, which was much larger than the conventional pinning size: the coherent length ξ. This effect could be attributed to a self-field, which was either generated by the current itself or by the applied magnetic field, penetrating into the defect smoothly and being pinned at the defect. A repulsive interaction between the self-field and the external field kept any further flux from abruptly penetrating into the junction. The increment in the critical current under the applied field was up to 125% of the original defect-free one. By fitting two defects of the same size of 2 λ_J and positioning them at 0.5 λ_J to both edges of the junction, the zero field critical current and the critical magnetic field were enhanced up to 150% of a defect-free junction.

1. Introduction

Recently, the grain boundary is found to be the major cause in limiting the transport current [1–4] and to be a source of noise [5]. The current density could be improved enormously by aligning the grain boundaries by the melt-texture technique [6,7] or by the directional phase transformation method [8]. The current density could even be raised up to a higher value by adding impurities [9–13]. It was believed that these additional impurities act as pinning centers. However, these pinning centers have sizes ranging from a few hundred Å to a few micrometers which are much larger than the expected pinning size of an order of the coherence length, ξ, in oxide superconductors. How such large impurities could act as pinning centers has not yet been understood. Intrinsically, these weak-link-like grain boundaries, or small angle grain boundaries, act as Josephson junctions. However, due to the complexity of grain boundaries [3,14], it is very difficult to describe the behavior of grain boundaries by ideal Josephson junctions. Moreover, some studies proposed that a grain boundary acts like the resistively shunted junction model [4,5] or a composition of many small junctions [14]. To understand the role played by grain boundaries, the single grain boundary or the junction made by the thin film technique on a bicrystal has been studied. The critical current density

* Corresponding author.

SSDI 0921-4534(95)00087-9

versus the applied magnetic field shows an ambiguous pattern that could only be intuitively related to the Fraunhofer pattern [4,14]. Obviously, no empirical model could be used to understand the fuzzy behaviors in a grain boundary or a realistic Josephson junction.

A realistic junction or grain boundary, which contains many defects or material inhomogeneity, complicates the behavior of the transport current in response to the applied magnetic field. Even though an extensive microscopic investigation of an ideal junction had been made by Owen and Scalapino [15] and Zharkov and co-workers [16–18], no experiments or theories could give a clear microscopic view to understand the complex behaviors in a real junction. To do so, we simplified a realistic Josephson junction by one that contains an antisymmetric point defect. Defects with various sizes were placed in different positions in the junction. The current and the applied magnetic field were then introduced upon the junctions. With most experimental techniques, the dynamics of the interaction between the transport current and the applied magnetic field during the experiment cannot be seen. To observe these dynamic pictures, the mechanical simulation is a very powerful tool. In the present experiment, we were able to observe the current distribution and the flux formation in the junction. In some cases, the field penetrated smoothly into the junction while, in most other cases, it formed a flux abruptly. The tunneling properties, the Fraunhofer pattern, were not influenced by the point defect that was located in the center of the junction unless it was moved to the edge of the junction. In some circumstances, a defect with a size of $2\lambda_J$ exhibited the strongest pinning effect that enhanced the critical current and the critical magnetic field.

2. Experiment

A mechanical simulation device was first developed by Yamashita et. al. [19] to study features of DC current versus magnetic field of a one-dimensional Josephson junction. A series of pendulums hanging vertically on a stretched rubber string were used to simulate a junction sandwiched by two superconductors on both sides. The DC current could

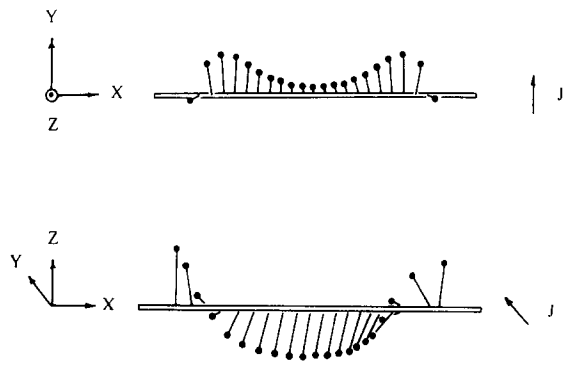

Fig. 1. The top view (a) and the side view (b) of the mechanical simulation of an ideal Josephson junction that carries a critical current under zero field.

be applied through the junction by rotating the rubber string in the same direction on both sides simultaneously. When both sides were rotated, a torque strain moved the hanging pendulums away from its vertical position at an angle. Gravity causes those pendulums on the edge swept faster than those in the center of the junction, as shown in Fig. 1. The vertical projection of the gravity torque on pendulums simulates the flow direction and the current density per unit length. The transport current prefers to pass through the edges than the center of the junction due to the Meissner effect. Therefore the mechanical pendulums' system can be regarded as equivalent to the Josephson junction not only in the current distribution but also in the mathematics. A certain degree of rotation on both sides of the rubber string corresponds to a constant applied DC current. As long as the transport current density is below the critical current density, one can visually see the stable tunneling current distribution on the string. When the applied current is stronger than the critical one, the pendulums on the edges will certainly flip over and form a vortex in the junction. Similarly, the external magnetic field can be simulated by rotating the rubber in opposite direction on both sides simultaneously, as shown in Fig. 2. A persistent super-current flows on both sides of the junction in the opposite direction to keep the inner junction in a pure Meissner state. To measure the critical current of the junction in different applied magnetic fields, we apply the magnetic field and follow by applying a current until visually recording the flip of the pendulum on either sides of the junction.

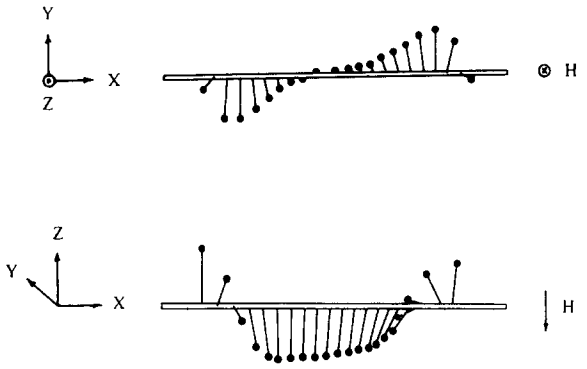

Fig. 2. The top view (a) and the side view (b) of the mechanical simulation of an ideal Josephson junction under the influence of a critical magnetic field.

In this setup, only the one-dimensional defect with a finite length smaller than the length of the junction will be created. To generate such defects, a few selected pendulums are replaced by lighter pendulums. Because the tunneling current corresponds to the vertical projection of the gravity torque of pendulums, a lighter pendulum with a small gravity torque represents a small tunneling current in the defect area. Therefore, the defect we introduced is different from an open defect in a tunneling junction. They are mostly like a hole of finite depth in the junction. The resistance to the tunneling current is stronger in the defected area than in the defect-free one. The junction would not be decoupled into two separate ones. This is the case similar to those additional impurities in the grain boundary, whose cross-sections are smaller than the area of grain boundaries. They do not cut the grain boundary into two separate ones but only form an obstacle for the current to flow by.

3. Results and discussion

The transport behavior of a Josephson junction of type-II superconductors under the influence of an external applied magnetic field are well described by three equations [20–22]. In a short junction, the critical current density varies with a weak magnetic field as a symmetric Fraunhofer pattern [23]. When the length of the junction is longer than 10 times the Josephson penetration depth, the Fraunhofer pattern stretches into different patterns as several overlapping triangles [24,25]. The solid line in Fig. 3 shows the first triangle which has no flux in it. In this ideal case, its critical transport current (I_C) is proportional to the reciprocal of the applied magnetic field (H). Inside this triangle, the junction exhibits nothing but a pure Meissner state. When point defects were introduced asymmetrically into the junction, the ideal pattern experienced a shift to a different position and became asymmetric. In Fig. 3, the point defect had a size of $2\lambda_J$. The pattern is changed according to the position of defects. When the defect was moved from the edge to the inner part of the junction, the triangular pattern was initially enlarged and then shrinked rapidly along one side of the triangle as shown by dashed lines. Finally, the pattern approached its original position whenever the center of the defect approached the center of the junction.

To understand the effect of defects on the critical current in the zero field (I_C^0) and the critical magnetic field (H_C^0), the I_C^0 and H_C^0 as a function of defect positions are plotted in Fig. 4. The position of the defect was measured from the edge of the junction to the nearest edge of the defect. Because the separation between pendulums was $0.5\lambda_J$, the horizontal axis was scaled to λ_J. Fig. 5(a) indicates a defect-free junction. The applied current flows by the

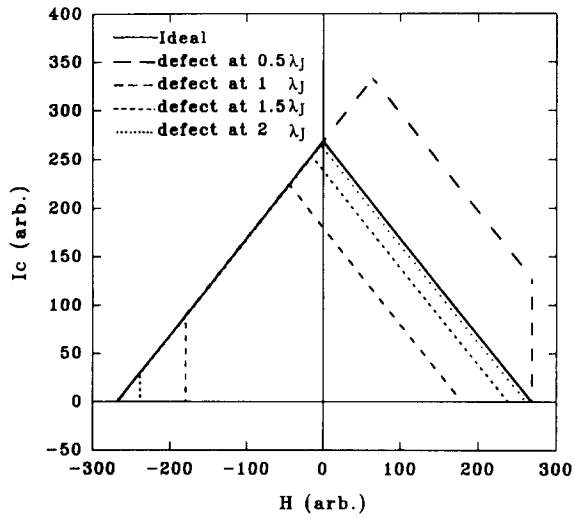

Fig. 3. The triangular patterns of long defected Josephson junctions with a defect whose size is $2\lambda_J$ and is located at different positions from the edge of junction.

two sides of the junction. The center of the junction remains at a pure Meissner state. The supercurrent remains in symmetric form if the defect sits at the center of the junction, Fig. 5(b). However, the symmetric distribution of the supercurrent is perturbed when the defect is located in a position that cuts into the area by which the current flows, as shown in Figs. 5(c) and 5(d). The defect forced a redistribution of this super-current. As a result, the completed Meissner area became shrunken or even disappeared. I_C^0 and H_C^0 decrease gradually to a minimum value when the defect approaches the edge of one λ_J, Fig. 5(d). Of course, the position of the defect was not the only source that influences I_C^0 and H_C^0; the size of the defect also affected them in other ways. Larger defects were more effective in affecting the current distribution. Therefore, the value of the critical current decreased faster for the junction containing larger defects.

A surprising result was observed when the defect was placed further outward to $0.5\lambda_J$. As shown in Fig. 3, I_C^0 and H_C^0 increase to that of a defect-free junction. We discovered that a small self-field, smaller than the field in one flux, which was generated by the applied current itself or the applied field penetrated smoothly into the defected area, also

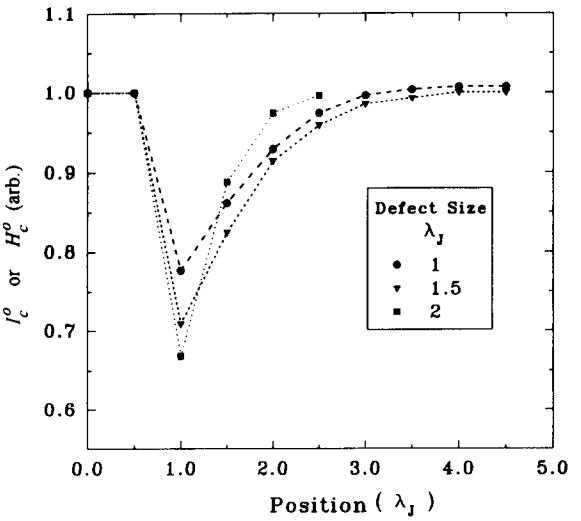

Fig. 4. The change of the zero field critical current density I_C^0 and the critical magnetic field H_C^0 as a function of defect positions with different defect sizes. The zero position indicates an ideal defect-free junction.

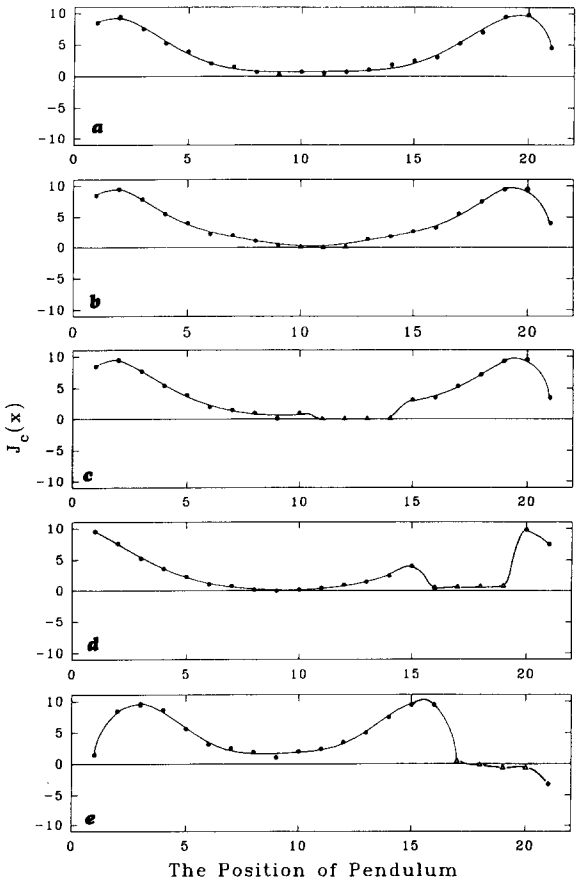

Fig. 5. The current distribution in Josephson junctions: (a) an ideal junction; (b) to (e) are defected junction for defects at different positions as shown in empty squares. The current distribution experiences a strong modulation when the defect approaches the edge of junction.

shown in Fig. 5(e). Even though the penetrated field was smaller than one flux, it acted as a pinned flux and resisted any further penetration of field to form a vortex in the junction. It was, therefore, necessary to apply a higher current to overcome this resistance to reach the critical current. Contrarily, the other side of the junction which was not defected, experienced no change at all. With the help of this resistant force the flux would no longer be able to penetrate into the junction from the defected side but from the defect-free side. I_C^0 and H_C^0 were then the same as if there were no defect. According to our results, this enhancement effect occurred only when defects were $0.5\lambda_J$ to $2\lambda_J$ in size and positioned at $0.5\lambda_J$ from the

edge of the junction. However, for those defects which were not in the special range, the flux preferred to penetrate abruptly into the junction.

The maximum critical current under the field, I_C^H, experienced a very similar enhancement effect when both the DC current and the external magnetic field were applied. In Fig. 6, I_C^H was plotted as a function of the defect size, and the different lines indicated different defect positions. For those junctions with the defect positioned at $0.5\lambda_J$, I_C^H dropped a little bit and then increased linearly up to its maximum value, 125% of I_C^0, when the defect changed in size from $0.5\lambda_J$ to $2\lambda_J$. We further enlarged the size of defects and an abrupt drop of I_C^H was observed, which remained decreasing. This strongly suggested that the penetrated field tended to be pinned at the defect as a flux. The stronger the pinning effect, the stronger the repulsive force was observed. The maximum value of I_C^H was found when the defect was $2\lambda_J$ in size, which was the space occupied by the magnetic field of a flux. Therefore, the penetrated field acted as a flux that could be pinned by a defect. In the case of a bulk system, it was believed that the strongest pinning effect was developed when the pinning center had a comparable size with the coherent length of a Cooper pair. Surprisingly, the penetrated field was found to be pinned to a much larger size, around 3

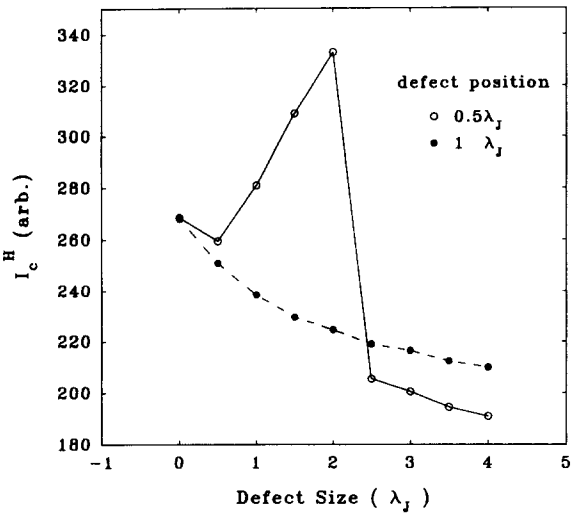

Fig. 6. The maximum critical current under the field is plotted as a function of defect sizes. The solid line and the dashed line are those defects located at 0.5 λ_J and 1 λ_J respectively.

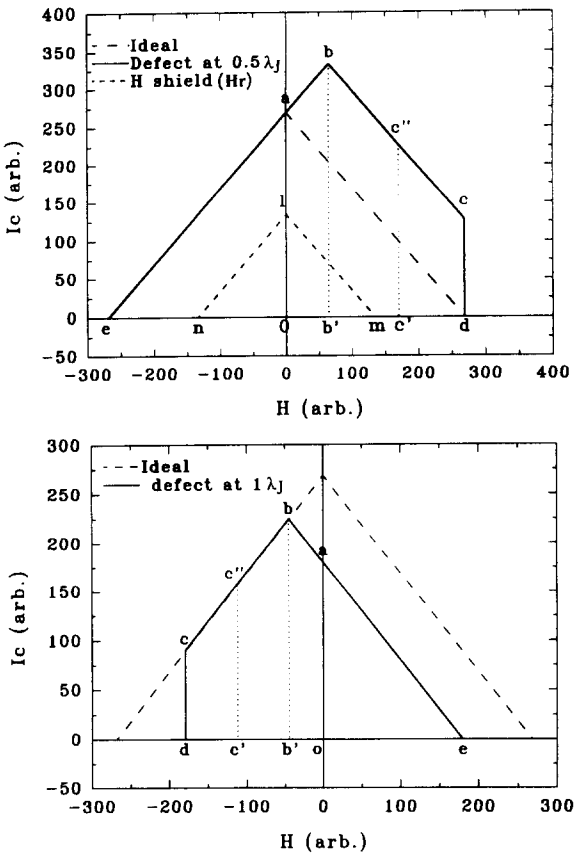

Fig. 7. The change of the triangular pattern due to the existence of a defect at different positions. The long-dashed triangle shows the behavior of an ideal Josephson junction. The solid one indicates the $I_C - H$ curve of a defected junction.

orders of magnitude larger than the coherent length. When the defect was smaller than $2\lambda_J$, the pinning size was not large enough to contain the entire penetrated field. Therefore, the pinning force was smaller and gave rise to a lower I_C^H. In opposite, the penetrated field was able to move freely inside defects larger than $2\lambda_J$, which resulted in lowering the repulsive force and I_C^H.

To understand the complete behavior of a defected junction, we have to know how the repulsive force acted and at which side of the junction the flux tended to penetrate first. Fig. 7 shows the patterns for a defect of size $2\lambda_J$ located at $0.5\lambda_J$ and $1\lambda_J$. The triangle *ead* is the first-order triangular pattern for an ideal long Josephson junction. The *ebcd* contour indicates a defected junction with the defect

located at $0.5\lambda_J$ and a size of $2\lambda_J$. To describe the situation qualitatively, we denote H^* to be the applied magnetic field, where the maximum I_C^H occurs, and H to be the external field we have applied. Because the defect-free side is kept at a long distance from the defect, it purely acts as an ideal junction. The critical field that needs to form a flux inside the junction from the defect-free side is denoted as $H_{c(n)}$. Neglecting the repulsive force between the penetrated field and the external field, the critical field $H_{c(d)}$ at the defected side becomes smaller than $H_{c(n)}$. The extra field that is needed to overcome the repulsive interaction is defined by H_r and is drawn as a short-dashed line in Fig. 7(a). When the penetrated field is pinned in the defect, H_r is stronger than $H_{c(n)} - H_{c(d)}$. To know how much current or applied magnetic field we really need, we define the equivalent fields, $H^e_{(d)}$ and $H^e_{(n)}$, to be the field required to overcome this barrier at the defected and the defect-free sides respectively.

To reach point a in Fig. 7(a), a DC current was supplied. The applied current flew through both sides of the junction initially. While more current was added, the defected side of the junction experienced a strong modulation. After the applied current exceeded the point l, the self-field started to penetrate into the defect smoothly. A repulsive interaction between the penetrated field and the external self-field was built up. Near point a, the defect-free side had reached its critical point (i.e. $H^e_{(n)} = H_{c(n)}$) and had readily been penetrated by a flux, while the defected side was still far away from its critical point (i.e. $H^e_{(d)} = H_{c(d)} + H_r > H^e_{(n)}$) because of the repulsive interaction. As long as the current reached the critical state, point a, the flux started to penetrate into the junction from the defect-free side. That was why, the critical current for a defect located at $0.5\lambda_J$ and with a size of $2\lambda_J$ was the same as an ideal junction.

To reach the point between a and b, a positive magnetic field was applied first and then a DC current was applied. In this simulation, a positive magnetic field means that the induced persistent current due to the applied field had the same direction as the applied current in the defected side, and, of course, had an opposite direction in the defect-free side. When a current was applied along a positive magnetic field, the distribution of current density in the defected side was strongly modulated by the superposition of both the persistent and the applied current (i.e. $H^e_{(d)} = H_{c(d)} - H + H_r$), while the other side experienced a cancellation effect (i.e. $H^e_{(n)} = H_{c(n)} + H$). This means that one needed to supply more current at the defect-free side to force a flux to go into the junction. Once the repulsive interaction (i.e. H_r) on the defected side was strong enough (i.e. $H_r > 2H + H_{c(n)} - H_{c(d)}$), the flux preferred to penetrate from the defect-free side rather than the other side. To reach the point between a and e, a negative magnetic field was applied instead, which caused a reverse effect to the one described above. The distribution of current density in the non-defect side was constructively superimposed. Between points a and e, the constructive superposition effect in the defect-free side was much stronger than the repulsive interaction in the defect side, and, the flux preferred to go into the junction from the defect-free side.

The point b in Fig. 7(a) was the place where the critical current under the field, I_C^H, experienced an enhancement over 125% of the original I_C^0. At this point, we simulated the process following the line $\overline{Ob'b}$ and observed an equal opportunity for both sides to be penetrated by flux. This enhancement effect in the defected side due to the repulsive interaction was balanced by the cancelation effect on the defect-free side ((i.e. $H_r = 2H^* + H_{c(n)} - H_{c(d)}$). Therefore, one needed a maximum current to force a flux into the junction.

Along the line $\overline{Oc'c''}$, a much stronger cancelation effect (i.e. $H^e_{(n)} = H_{c(n)} + H$) occurred on the defect-free side and a stronger current was needed to overcome this effect so as to force the flux through this side. On the other side, the defected side, the applied field enhanced the current density too much (i.e. $H_r < 2H + H_{c(n)} - H_{c(d)}$) that it weakened the resistance (i.e. $H^e_{(d)} = H_{c(d)} - H + H_r$) to the flux. In this way, a flux penetrated from the defected side and led to a lowering of the critical current of the junction. Following the path $\overline{Odc}$, we found that we were not able to reach point c. Because the point d had a magnetic field with the same magnitude as that of the point e, the junction acted as along the $\overline{Oe}$ path. The flux penetrated from the defect-free side, and the defected junction transformed to the second phase with a vortex in the junction.

If one moved the defect to the inner part of the

junction, the repulsive interaction was totally eliminated as shown in Fig. 7(b) in which the short-dashed triangle no longer existed. To reach point a in Fig. 7(b), both the defected and defect-free side needed to be supplied with equivalent fields $H_{c(d)}$ and $H_{c(n)}$ respectively. For $H_{c(d)}$ smaller than $H_{c(n)}$, the flux penetrated into junction from the defected side as expected. Along line $\overline{ae}$, a positive magnetic field was applied and strongly modulated the current distribution (i.e. $H^e_{(d)} = H_{c(d)} - H$) in the defected side. The other side experienced a cancelation effect (i.e. $H^e_{(n)} = H_{c(n)} + H$). Therefore, the flux penetrated from the defected side. In another line $\overline{ab}$, the negative magnetic field ($|H| = H$) exhibited a cancellation effect in the defect side (i.e. $H^e_{(d)} = H_{c(d)} + H$) and an enhancement effect in the defect-free side (i.e. $H^e_{(n)} = H_{c(n)} - H$). The flux penetrated into the junction from the defected side as far as point b where $H_{c(n)} - H_{c(d)} = 2H^*$ was reached. By inspecting Fig. 3, point b was moving closer to the tip of an ideal junction when the defect was moving to the inner part of the junction. It was clear that the properties of both sides became more similar as expected when the defect moving inward. Along $\overline{bc}$, the magnetic field was stronger than H^* such that the flux penetrated from the defect-free side instead. Similar to points c and d in Fig. 7(a), we were not able to reach point c but point d.

It was interesting to know if we can increase I_C^0 and H_c^0 by introducing two similar defects on both sides of the junction. As expected, I_C^0 and H_c^0 could be enhanced by 150% of the defect-free value as shown in Fig. 8.

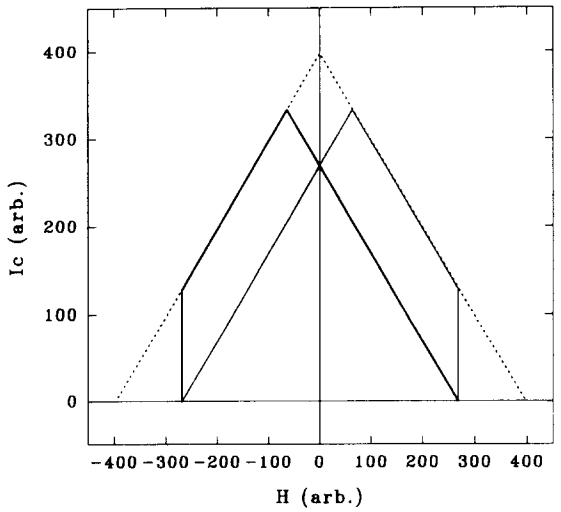

Fig. 8. The ideal triangle of an ideal junction could be symmetrically enhanced by introducing two defects with the same size and with the same distance from both sides of the junction. The enhancement was observed to go up to 150% of the original value.

4. Summary

A defect in a Josephson junction was simulated by switching pendulums to the ones with smaller torque in a mechanical simulation. As long as the defect did not decouple the junction into two separated ones, the influence of the defect was tremendous. It was found that the self-field due to the applied current or the magnetic field tended to penetrate smoothly into the defect when the defect was placed at $0.5\lambda_J$ from the edge of the junction. Inside the junction, a strong pinning force happened when the defect had sizes ranging from $0.5\lambda_J$ to $2\lambda_J$ which was 3 orders of magnitude larger than the conventional pinning size, ξ, in the bulk superconductor. The penetrated field interacted with the external field and resulted in a repulsive force to keep the flux away from the junction in the defected side. The critical current under field, I_C^H, was enhanced up to 125% of the original defect-free one. When the defect moved toward the center of the junction, the external field no longer penetrated into the junction smoothly but abruptly and the modulation effect on the current which flew through the defected side declined. With a careful design, we were able to increase the critical current at zero field, I_C^0, and the critical field, H_c, to 150% of the defect-free one by placing two defects of $2\lambda_J$ in size at $0.5\lambda_J$ from both edges of the junction.

Acknowledgements

This project was supported by the National Science Council in Taiwan.

References

[1] P. Chaudhari, J. Mannhart, D. Dimos, C.C. Tsuei, J. Chi, M. Oprysko and M. Scheuermann, Phys. Rev. Lett. 60 (1988) 1635.

[2] S.E. Babcock, X.Y. Cai, D.L. Kaiser and D.C. Larbalestier, Nature 347 (1990) 167.
[3] D. Dimos, P. Chaudhari and J. Mannhart, Phys. Rev. B. 41 (1990) 4038.
[4] M. Daumling, E. Sarnelli, P. Chaudhari, A. Gupta and J. Lacey, Appl. Phys. Lett. 61 (1992) 1355.
[5] R. Gross, P. Chaudhari, D. Dimos, A. Gupta and G. Koren, Phys. Rev. Lett. 64 (1992) 228.
[6] S. Jin, Mater. Sci. Eng. B 7 (1991) 143.
[7] D. Shi, S. Sengupta, J.S. Luo, C. Varanasi and P.J. McGinn, Physica C 213 (1993) 179.
[8] V. Selvamanickam, A. Goyal and D.M. Kroeger, Appl. Phys. Lett. 65 (1994) 639.
[9] M. Murakami, M. Morita and N. Koyama, Jpn. J. Appl. Phys. 28 (1989) L1125.
[10] M. Murakami, Mod. Phys. Lett. 4 (1990) 163.
[11] S. Pinol, F. Sandiumenge, B. Martinez, V. Gomis, J. Fontcuberta, X. Obradors, E. Snoeck and Ch. Roucau, Appl. Phys. Lett. 65 (1994) 1448.
[12] J.C.L. Chow and P.C.W. Fung, Chem. Phys. Lett. 223 (1994) 185.
[13] K. Osamura, T. Kizu and T. Oku, Physica C 226 (1994) 113.
[14] C. Sarma, G. Schindler, D.G. Haase, C.C. Koch, A.M. Saleh and A.I. Kingon, Appl. Phys. Lett. 64 (1994) 109.
[15] C.S. Owen and D.J. Scalapino, Phys. Rev. 164 (1967) 538.
[16] S.A. Vasenko and G.F. Zharkov, Sov. Phys. JETP 48 (1978) 89.
[17] G.F. Zharkov, Sov. Phys. JETP 44 (1976) 1023.
[18] G.F. Zharkov and S.A. Vasenko, Sov. Phys. JETP 47 (1978) 350.
[19] K.I. Yoshida and K. Hamasaki, J. Appl. Phys. 49 (1978) 4468.
[20] B.D. Josephson, Phys. Lett. 1 (1962) 251.
[21] B.D. Josephson, Rev. Mod. Phys. 36 (1964) 216.
[22] B.D. Josephson, Adv. Phys. 14 (1965) 416.
[23] P.W. Anderson and J.M. Rowell, Phys. Rev. Lett. 10 (1963) 230.
[24] L. Solymar, Superconductive Tunnelling and Application (Chapman and Hall, London, 1972).
[25] R.A. Ferrel and R.E. Prange, Phys. Rev. Lett. 10 (1963) 479.